SEDIMENTOLOGY the journal of the International Association of Sedimentologists

Sedimentology (2014) **61**, 1793–1811 doi: 10.1111/sed.12116

Sediment colour reflectance spectroscopy as a proxy for wet/dry cycles at Lake El'gygytgyn, Far East Russia, during Marine Isotope Stages 8 to 12

JEREMY H. WEI*, DAVID B. FINKELSTEIN*, JULIE BRIGHAM-GRETTE*, ISLA S. CASTAÑEDA* and NORBERT NOWACZYK†

**Climate Systems Research Center and Department of Geosciences, University of Massachusetts Amherst, Amherst, MA 01003 (E-mail: jeremyhcwei@gmail.com)*

†Helmholtz Centre Potsdam, GFZ German Research Centre for Geoscience, Section 5·2, Climate Dynamics and Landscape Evolution, Telegrafenberg, C 321, D-14473 Potsdam, Germany

Associate Editor – Daniel Ariztegui

ABSTRACT

Marine Isotope Stage 11 has been proposed as an analogue for the present interglacial interval; yet, terrestrial climate records from both this region and time interval are rare. The sediments deposited at Lake El'gygytgyn (67°30′N, 172°5′E) in Far East Russia contain a 3·56 Ma record of climate variability. This study presents a high-resolution record of sediment colour change from Marine Isotope Stage 8 to 12 (*ca* 275 to 475 ka) and demonstrates the link between lake catchment processes and climate variability. The hue colour parameter, calculated from data collected via colour reflectance spectroscopy in the visible spectrum (380 to 720 nm), exhibits correspondence with global climate records. Determining the source of sediment colour changes was achieved through detailed mineralogical and sedimentological methods, and linked to colour changes through a series of colour sensitivity tests. Mineralogical data, measured by X-ray diffraction, reveal fluctuations in concentrations of clay minerals corresponding to colour changes. Further analyses of the clay mineral assemblages show no change in relative clay mineral abundances, yet demonstrate a lake catchment dominated by physical weathering processes. Using measured mineral abundances, reconstructions of sediment colour based on colour reflectance mineral standards link mineral and clay mineral content to overall sediment colour. Colour sensitivity tests demonstrate the ability of iron oxide minerals to stain sediments red. Additionally, colour sensitivity to organic matter content was tested, suggesting that organic content drives variability in the red portion of the spectrum and darkens the overall colour signal. Sediment colour is then ultimately linked to physical weathering of bedrock minerals, with small amounts of chemical weathering producing iron oxides during wet intervals. Fluctuations in the sediment colour reveal a high-resolution record of wet/dry cycles, and provide new information about wet periods for the Russian Arctic region not yet understood from other lake proxy records.

Keywords Clay mineralogy, colour reflectance spectroscopy, high-resolution proxy, Lake El'gygytgyn, palaeoclimate.

INTRODUCTION

Marine Isotope Stage (MIS) 11 has been proposed as an analogue to modern climate conditions, with orbital configurations similar to today and greenhouse gas concentrations at pre-industrial levels (Loutre & Berger, 2002; EPICA Community Members, 2004). Past studies indicate that MIS 11 was one of the warmest and longest interglacial periods of the past 3 Ma, with the characteristics of this 'super' interglacial (Melles *et al.*, 2012) period expressed globally in ice cores from Antarctica (EPICA Community Members, 2004), North Atlantic marine sediment core records (Lawrence *et al.*, 2009), as well as in Asian lacustrine sedimentary records from Lake Baikal, which indicate a prolonged interglacial period of *ca* 30 ka (Prokopenko *et al.*, 2010). However, long terrestrial records from high latitude regions of the Asian continent are almost non-existent, yet can play a crucial role in understanding aspects of the Northern Hemisphere climate system and hemispheric teleconnections. The sediment record obtained from Lake El'gygytgyn in Far East Arctic Russia (Fig. 1) contains a continuous archive of climate variability since the middle Pliocene, and permits critical analysis of the structure and corresponding response of this western Beringian lake system to changes during the MIS 11 'super' interglacial period.

The interval spanning MIS stages 8 to 12 is of particular interest to palaeoclimatic studies because higher magnitude glacial–interglacial transitions, such as the MIS 12 to MIS 11 (Termination V) transition, were comparatively larger than previous glacial–interglacial transitions (EPICA Community Members, 2004). During the peak warmth of MIS 11, global sea-level is thought to have been significantly higher than other interglacials over the past 400 kyr, possibly due to significant collapse of both the Greenland Ice Sheet and the West Antarctic Ice Sheet (Raymo & Mitrovica, 2012). This interval, known as the Mid-Bruhnes transition, marks a period when the amplitude of interglacial–glacial variability increases after *ca* 430 ka. Furthermore, past studies on Lake El'gygytgyn sediments by

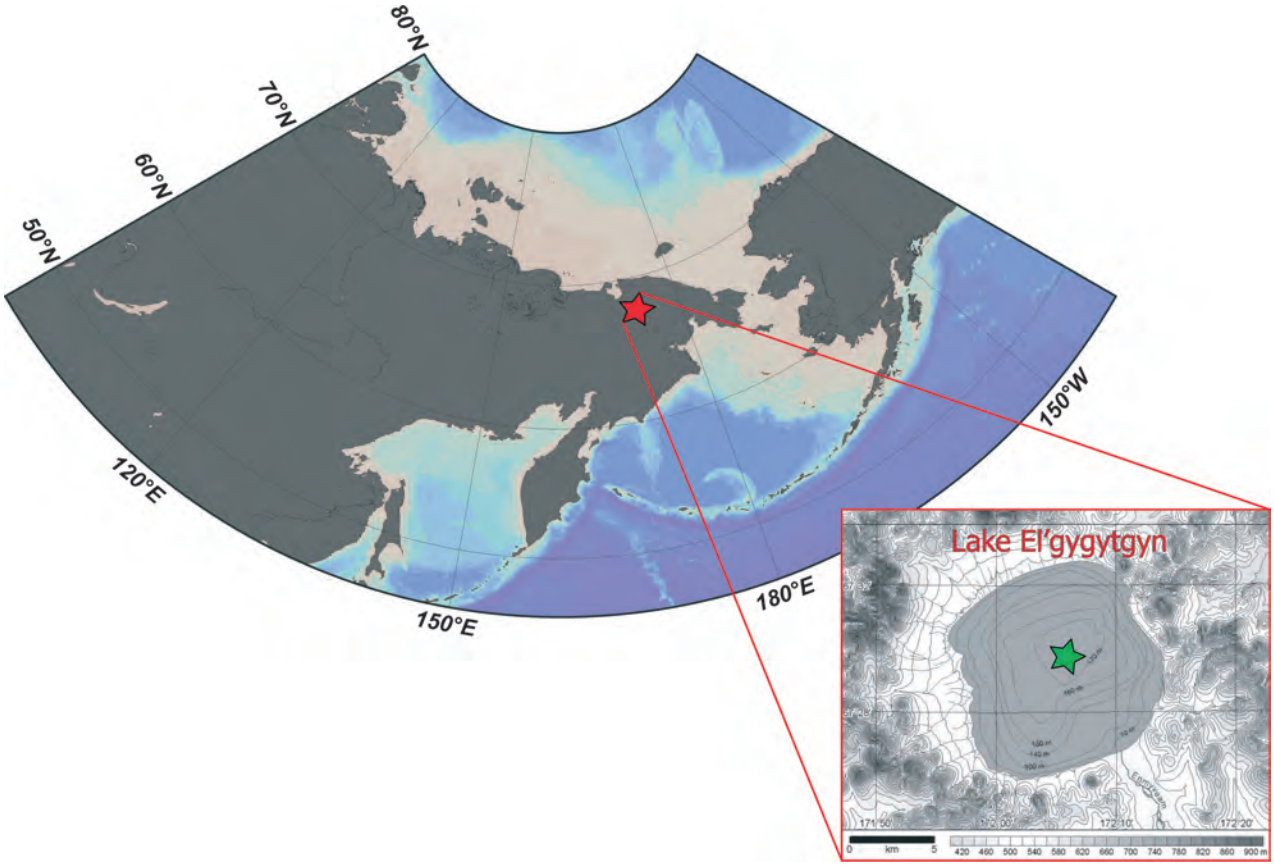

Fig. 1. Location of the lake (red star), as well as an inset map marked with the position of the ICDP core 5011-1 (green star).

Melles *et al.* (2012) classify MIS 11c as a 'super' interglacial where lake sediments reflect high diatom and terrestrial plant productivity. Biomarker investigations by D'anjou *et al.* (2013) demonstrated elevated terrestrial and aquatic productivity at Lake El'gygytgyn during the interglacial period, as well as during MIS 9. Additional work in this lake system confirms a shift towards warmer conditions during MIS 11 (Vogel *et al.*, 2013); however, further analysis is needed to understand more completely interglacial–glacial changes and the effects on lake processes.

The present study focuses on validating the use of colour spectroscopy as a potential proxy for changes during the MIS 8 to 12 interval, as well as testing the viability of the colour record in other portions of the sediment record. Colour properties, measured by colour reflectance spectroscopy, include the hue colour parameter (Nowaczyk *et al.*, 2013), which suggests a remarkable correspondence to global climate proxies, such as global benthic foraminifera records (Lisiecki & Raymo, 2005; $r^2 = 0{\cdot}58$, n = 239; Fig. 2). The physical connection of the hue record to lake sedimentological dynamics and processes, however, is not yet understood, and past work involving mineralogy (Asikainen *et al.*, 2007; Minyuk *et al.*, 2013; Wennrich *et al.*, 2013) did not cover the MIS 8 to MIS 12 time interval where two of these 'super-interglacial' sediment facies exist (Melles *et al.*, 2012). By classifying the bulk and clay mineral components of the

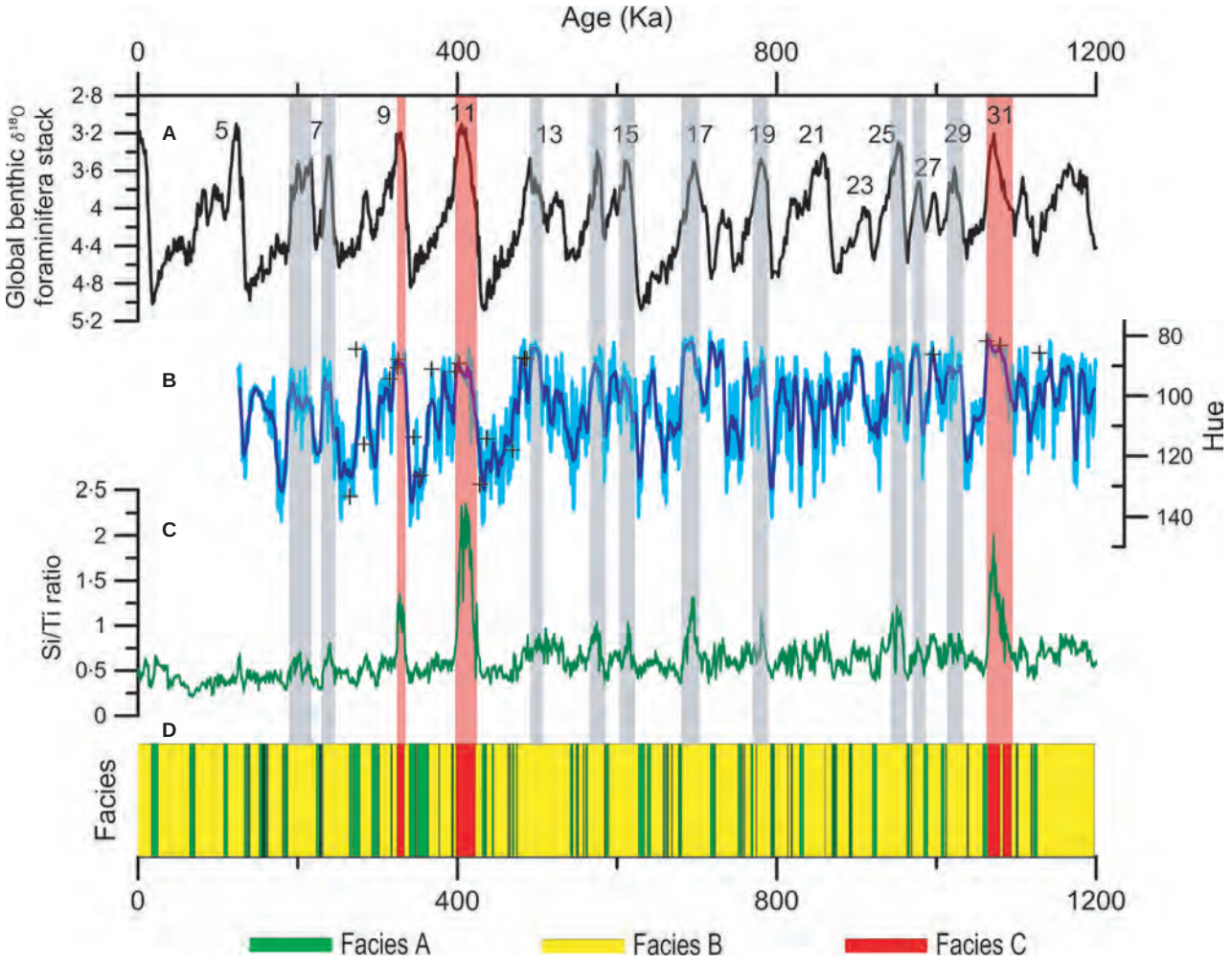

Fig. 2. Comparison of the global benthic $\delta^{18}O$ foraminifera stack (Lisiecki & Raymo, 2005; black line), the Lake El'gygytgyn hue colour record (blue line, 11 pt running average), the Si/Ti ratio, which is a proxy for diatom productivity (green line; Melles *et al.*, 2012) and the facies interpretations assigned by Melles *et al.* (2012) for the sediment record. Interglacial Marine Isotope Stages are labelled according to Lisiecki & Raymo (2005), red shading indicates correlations of MIS 9, MIS 11 and MIS 31, and grey shading indicates interglacials recorded in both the benthic foraminifera and the hue colour record. Black crosses represent the ages of the 20 samples analysed for this study.

MIS 8 to 12 sediment, which includes all three sediment facies (glacial, interglacial and super interglacial – described below) found throughout the core, sediment mineralogy and components have been linked to rapid core scanning techniques. Building on past studies that have demonstrated how sediment mineralogy, clay minerals and other properties can drive sediment colour changes (Ortiz *et al.*, 2009; Trachsel *et al.*, 2010), the present study demonstrates the link between sediment mineralogy and colour by directly comparing X-ray diffraction (XRD) mineral analyses with investigations of the visible colour spectral data and the calculated first derivative spectra (Barranco *et al.*, 1989). In addition to XRD mineral analysis, further calibration tests, specifically designed to understand the relations between organic content and Fe-oxide minerals, were conducted to explain more completely the relation between lake catchment processes, sediment facies and the colour of the Lake El'gygytgyn sediments. By incorporating both mineralogical and colour sensitivity tests, colour reflectance spectroscopy is shown to validate sediment colour as a proxy for environmental changes in Lake El'gygytgyn, and demonstrates the potential utility of this method for sedimentary systems.

BACKGROUND AND SETTING

Lake El'gygytgyn is located on the Chukotka Peninsula in the Far East Russian Arctic (67°30′N, 172°5′E) (Fig. 1). The catchment area sits within an impact structure formed at 3·58 ± 0·04 Ma (Layer, 2000), with a rim to rim diameter of 18 km and a catchment area of *ca* 293 km^2 (Nolan & Brigham-Grette, 2007). A network of 50 small streams carries surface runoff into the lake, and the Enmyvaam River serves as the outlet to the Bering Sea (Nolan & Brigham-Grette, 2007). Lake El'gygytgyn is 12 km wide and 175 m deep with an approximate volume of 14·1 km^3 (Nolan & Brigham-Grette, 2007; Fig. 1).

The bedrock geology of the surrounding catchment is dominated by a range of andesitic to rhyolitic rocks, consisting primarily of ignimbrites and tuffs of the Pykarvaam and Ergyvaam Formations (Belyi & Raikevich, 1994) and, to a lesser extent, the Voronian Formation (ignimbrites and tuffs) and Koekvun' Formation (andesite-basalts, tuffs and tuffaceous sands) (Belyi & Raikevich, 1994; Belyi & Belaya, 1998; Minyuk *et al.*, 2013).

Modern precipitation levels are generally low, with cumulative precipitation from 2002 to 2007 ranging from 70 to 200 mm (Nolan, 2013). Strong winds also affect the El'gygytgyn area, with dominant directions out of the north or south and the strongest winds during winter (Nolan & Brigham-Grette, 2007). The Lake El'gygytgyn region is located in an area of continuous permafrost, with erosion and sediment transport mechanisms dominated by weathering related to permafrost activity (Schwamborn *et al.*, 2008). The modern vegetation around the lake can be characterized as arctic tundra consisting of lichen and herbaceous taxa (Lozhkin *et al.*, 2007). Around the high-relief slopes of the catchment basin this flora is often limited and discontinuous. The closest modern day light conifer forests lie *ca* 150 km south-west of the lake (Lozhkin *et al.*, 2007).

FACIES DESCRIPTIONS

The three sediment facies describe three separate types of sedimentation; descriptions were based on numerous parameters, such as colour, grain-size and sedimentary structures (Melles *et al.*, 2012). Facies A represents colder, glacial intervals characterized by dark grey/green sediment, with fine clay laminations and the smallest grain-sizes. Facies B is the most common, with colour ranging from grey to red and predominantly massive sedimentation during interglacial intervals. Transitions between Facies B and other facies are typically gradational in nature. Facies C occurs only during the warmest interglacial periods, and is distinguished by its red sediment colour, as well as fine laminations distinct from those found in Facies A (Fig. 3).

CHRONOLOGY

Sediment used by this study was taken from International Continental Scientific Drilling Program (ICDP) core 5011-1, extracted from Lake El'gygytgyn in spring 2009. Sixteen samples were taken at varying composite depth intervals between 13·9 m and 20·7 m, with each sample representing *ca* 250 to 500 years. The composite core record (Wennrich *et al.*, 2013) was tuned using tie points based on palaeomagnetic investigations and the ages of oxygen isotope intervals from Lisiecki & Raymo (2005), who reported an error of 4 ka for the 0 to 1 Ma

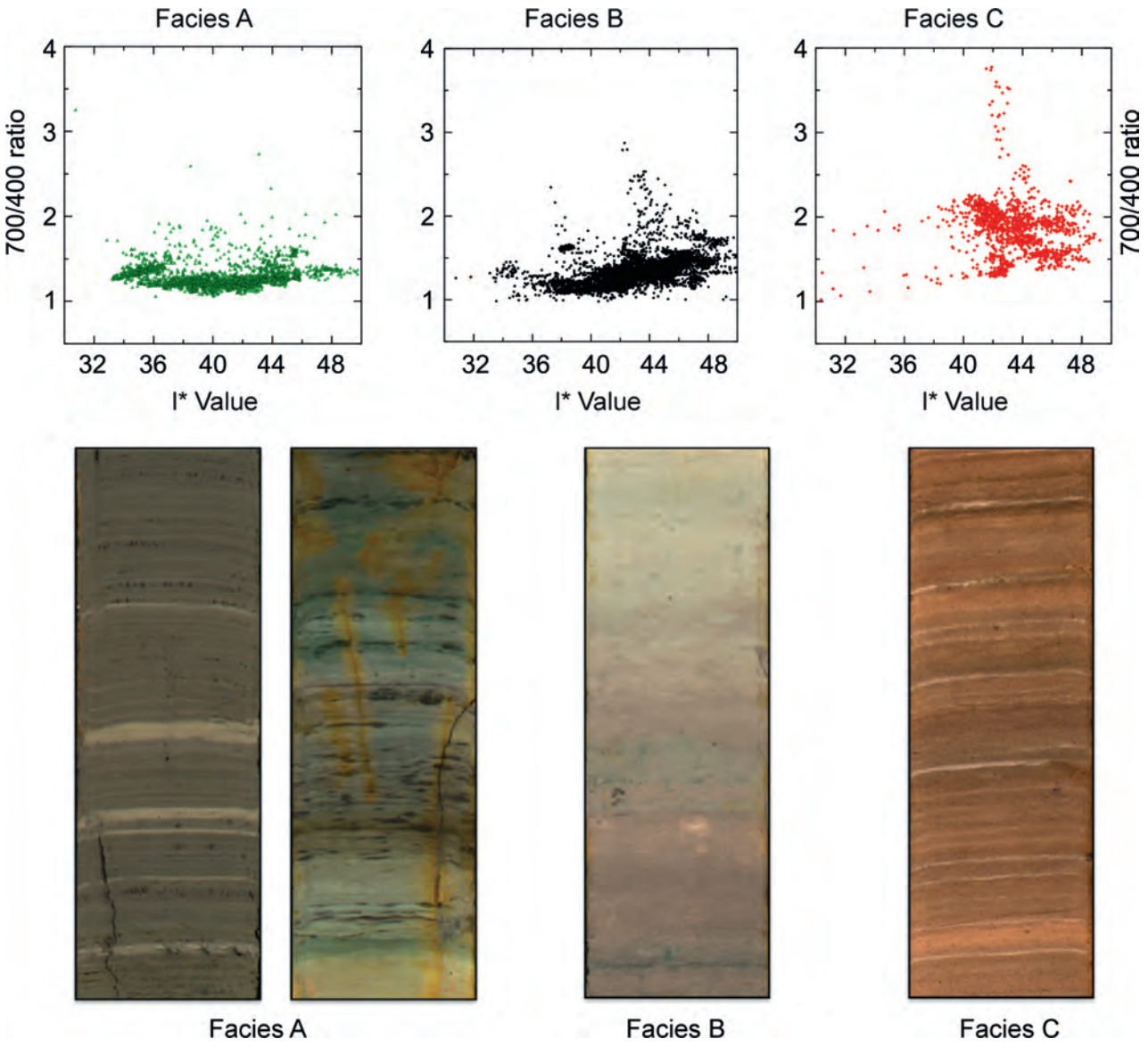

Fig. 3. Representative images of the three sediment facies, as described in Melles *et al.* (2012), as well as the Q7/4 diagram (Debret *et al.*, 2011) for individual facies (plotted with the same x, y axis values). The Q7/4 plots the ratio of the 700 to 400 nm wavelength band with the L* reflectance parameter. Facies A consists of dark grey/green sediments deposited during glacial intervals, with a relatively wide range of L* values but consistent 7/4 ratios. Facies C is distinguished by its red colour and fine laminations, higher L* values, as well as a wider range of 7/4 ratio values, while Facies B is composed of massive, olive grey to reddish brown sediments, which plot in between the Facies A and C end members on the Q7/4 diagram.

interval. This work and synchronous tuning of nine data sets between the palaeomagnetic tie points were first reported in Melles *et al.* (2012).

COLOUR PROXIES AND ANALYSIS

Colour parameters, analysed in previous studies (Debret *et al.*, 2011), provided the framework for this research. The present study utilizes the hue colour parameter, calculated from the CIE (International Commission on Illumination) L*, a*, b* colour parameter, and defined as Hue = atan2 (b*, a*) (Nowaczyk *et al.*, 2013). Colour parameters were measured using colour reflectance spectroscopy, which is a rapid and non-destructive core scanning technique. Other studies have used the CIE L*, a*, b* colour

parameters to track changes in sediment colour due to changes in monsoon conditions in Asia (Ji *et al.*, 2005), or to detect millennial-scale changes in the North Atlantic ice-rafted debris (Helmke *et al.*, 2002), alongside a variety of other sedimentary applications in other ocean basins (Mix *et al.*, 1992; Moy *et al.*, 2002; Debret *et al.*, 2006; Deplazes *et al.*, 2013). The hue colour parameter can be used as a measurable parameter from sediment cores, especially when used in conjunction with analysis of both the visible spectra (VIS) and first derivative spectra (FDS). The VIS and FDS colour continuums provide a qualitative estimate of different mineral types within the sediment (Barranco *et al.*, 1989), with distinctive patterns identified for iron hydroxide minerals (Deaton & Balsam, 1991; Debret *et al.*, 2011), as well as organic material and pigment compounds (Von Gunten *et al.*, 2009, 2012). When paired with mineralogical analysis and identification, the visible and derivative spectra can link mineralogy and colour visible measurements, such as hue, and allow for the rapid, non-destructive analysis of sediment core data (Ortiz *et al.*, 2009; Trachsel *et al.*, 2010).

METHODS AND MATERIALS

Clay methods

Sub-sampling of the core material was carried out at the University of Cologne, Germany. Facies specific samples were obtained, with *ca* 5 g samples taken for clay mineralogy every 1 cm for selected intervals of the core. In total, 16 samples from the MIS 8 to 12 interval, as well as four samples from MIS 31 were analysed for mineralogy and colour signals.

Analysis of clay minerals utilized the filter transfer method (Moore & Reynolds, 1997), with samples processed and analysed using a Philips X-ray diffractometer (CuKa radiation; PANalytical BV, Almelo, The Netherlands). Approximately 2 g of each sample was broken up and then sonicated for 30 min in 25 ml of water. Following sonication, each sample was centrifuged at 1500 rpm for 45 sec for the separation of the <2 μm fraction and 22 min for the <0·02 μm fraction. The supernatant was removed; each supernatant was vacuum filtered through Millipore® 0·22 μm filters and then transferred to a petrographic microscope slide. Although the filter pore size is larger than the 0·02 μm clay fraction, flocculation of the clay minerals effectively 'clogs' the filter, allowing for the accumulation of oriented clay. Oriented slides were produced by carefully transferring the sediment collected on the filter paper to a cleaned slide; the sediment was then left to dry.

For XRD analysis of the oriented clay slides, air-dried samples were scanned from 2° to 35° 2θ with a step size of 0·04° 2θ, at 0·5 sec intervals for each step under a 1·541874 Å CuKa beam, and with a tension of 45 kV and an amperage of 40 (units) as in Asikainen *et al.* (2007). Following analysis, each sample was then treated with an ethylene glycol-solvation to test for expandable layer clay minerals. Bulk weight percentages were calculated based on relative peak heights. Clay mineral abundance was calculated from the ethylene glycol-solvated XRD pattern using peak areas and mineral intensity factors from Reynolds (1989). The interlayer ordering and abundance of expandable layers in mixed-layer clays were determined by comparing the observed ethylene glycol-solvated pattern to XRD patterns calculated by the NEWMOD computer program (Reynolds, 1985) and by the peak position of the 001/002 versus 002/003 (Reynolds, 1980).

Additional analysis of clay polytypes was carried out by measuring the 2θ angle range from 30° to 45° 2θ. Diagnostic peaks for chlorite polytypes (Brown & Bailey, 1963) were used for polytype peak identification.

X-ray diffraction mineral analysis

Analyses were performed on packed powder mounts using a programmed continuous scan from 5° to 65° 2θ, a step size of 0·04° and a count time of 3 sec with the same CuKa parameters discussed above. For both bulk minerals and clay minerals, identification was based on multiple (five or more) peaks, and weight percentages were calculated using peaks unique to individual minerals (Fig. 4). Mineral abundance was calculated using the area of selected peaks and mineral intensity factors from Hoffman (1976) and Bayliss (1986). X-ray diffraction determinations of mineral abundance have errors of ±10% of the amount present for samples with a similar mineralogy (Bayliss, 1986). Mineral abundance was calculated using the area of selected peaks and mineral intensity factors from Bayliss (1986). The 2 μm size fraction was analysed to maximize the intensities of the detrital signature of the clay minerals and was comprised of kaolinite, illite

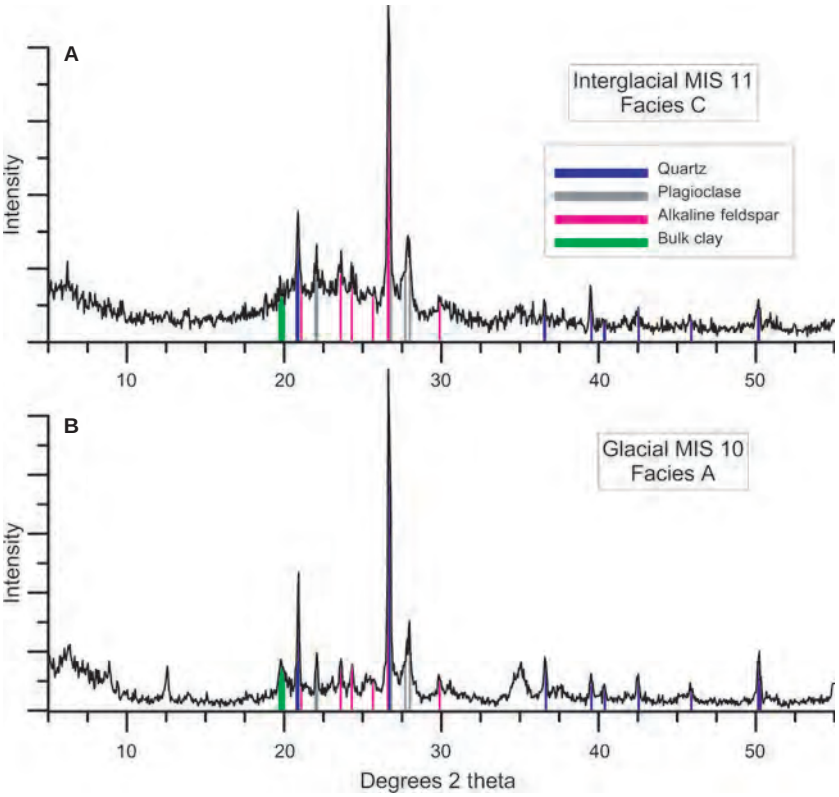

Fig. 4. Representative bulk XRD diffractograms for both an interglacial and glacial samples. Peaks used for major mineral identification are coloured for quartz (blue), plagioclase (grey), alkaline feldpsars (magenta) and the shared bulk clay peak (green).

and chlorite, rather than the <1 μm size fraction which was dominated by interlayered illite/smectite (I/S) and smectite (Gibbs, 1977; Brown & Brindley, 1980).

Grain-size analysis

Grain-size analyses were carried out using a Coulter LS 200 Laser particle size analyzer (Beckman Coulter Inc., Brea, CA, USA). This instrument measures the volume per cent of selected bin sizes, which ranges from 0·488 to 2000 μm grain-sizes (Sutinen *et al.*, 1993). Prior to processing, samples were treated with 10 ml 30% H_2O_2 to remove organic content, 8 ml of 0·5 M HNO_3 to remove diagenetic vivianite crystals and 10 ml of 1 M NaOH to remove biogenic silica for each *ca* 1·5 g sample, following the methods in Asikainen *et al.* (2007).

Colour reflectance spectrophotometry

Raw colour spectrum data were obtained by Nowaczyk *et al.* (2013) at AWI in Potsdam, Germany. A Gretagmacbeth Spectrolino™ spectrophotometer (XRite GmbH, Munich, Germany) mounted on a specialized core scanning track obtained a full visible colour spectrum from 380 to 720 nm at a physical resolution of 10 nms (36 bands), with a colour measurement taken every 1 mm. The instrument has a 4 mm diameter window, and utilizes a centre weighted measurement technique. In addition to raw reflectance data, CIE L*, a*, b* values were obtained. The hue value was calculated from the a* and b* values, and is defined by the equation Hue = atan2 (b*, a*).

Processing of the raw colour data was carried out with MatLab computer scripts written to calculate specific colour parameters. First derivative spectra data (FDS values; Barranco *et al.*, 1989; Deaton & Balsam, 1991; Balsam & Beeson 2003) were also calculated from the raw visible spectra data.

To validate mineralogy and colour continuums, mineral reflectance standards were downloaded from the US Geological Survey (USGS) Spectral Library (Clark *et al.*, 2007), and VIS and FDS continuums were calculated for each mineral. Based on mineralogical identifications performed by XRD analysis, USGS standards for the minerals quartz, albite, anorthite and orthoclase, as well as the clay minerals chlorite, illite and smectite were obtained (Fig. 5). Based on bulk mineralogy results from XRD analysis, colour continuums for sediments were constructed

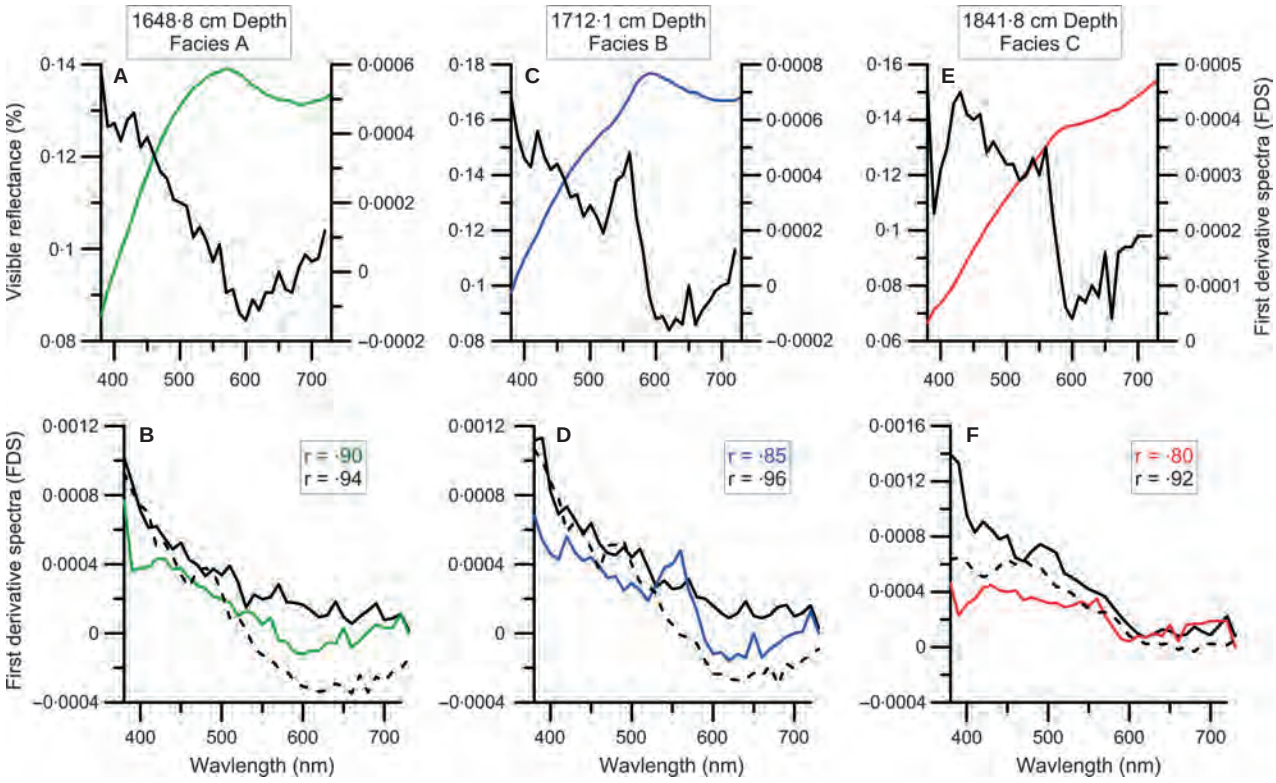

Fig. 5. The three top plots demonstrate VIS (coloured) and FDS (black) plots for selected samples representing the three sediment facies. The three bottom plots show calculated FDS values for the core measurements (black), the reconstructed FDS based on mineralogy (coloured) and FDS calculated post-iron digestion (dashed black). *R* values compare the correlations between measured FDS and reconstructed (coloured *r* values), as well as the correlations between reconstructed and post-iron digestion analysis (black *r* values).

using standards and mineral abundances (wt%), and then compared with measured VIS and FDS components. Correlation (*r*) values for each of the 20 sediment samples were calculated to test whether the minerals present were the dominant source of the colour signals.

Colour sensitivity tests

Additional techniques were utilized to determine the relative effects of Fe-oxide and hydroxide minerals as well as organic content on sediment colour reflectance measurements. Because Fe minerals are insensitive to the Cu radiation used by XRD analysis, other methods of mineral analysis were necessary. To test the colour signal attributed to iron oxide minerals, additional investigations using scanning electron microscopy (SEM) and iron oxide digestions were performed.

For SEM analysis, thin sections obtained from all three described sediment facies were analysed with a Zeiss EVO 50 SEM (Carl Zeiss Microscopy GmbH, Jena, Germany), with images and elemental [energy dispersive spectrometry (EDS)] data obtained for a suite of mineral grains in each thin section.

For colour sensitivity measurements, samples were filtered onto 0·2 μm filter papers, with colour measured on filtered wet sediments using a Konica Minolta 2600d spectrophotometer (Konica Minolta Inc., Tokyo, Japan) both prior to and following the iron digestion. Special care was taken to measure each sample before drying, because Balsam *et al.* (1998) found that progressively drying samples increased the brightness of sediment (higher reflectances) with time.

An iron oxide digestion protocol utilizing a citrate–bicarbonate–dithionite treatment was applied to the sediment samples. Approximately 2·5 g of sediment was digested according to the treatment (Jackson, 1969) for all 20 sediment samples. To test the effect of iron oxide on sediment colour, spectral measurements obtained following Fe-oxide digestion were correlated with the artificially constructed colour spectra,

Table 1. Breakdown of various data measurements by the facies description of Melles *et al.* (2012). See text for detailed descriptions of various measured parameters.

Composite depth (cm)	Age (ka)	Facies	Clay (%)	Quartz (%)	Calculated versus measured FDS	Calculated versus Fe digested FDS	Hue (degrees)	Fe solution data (wt%)	Mn solution data (wt%)	Water content (%)
1379·5	283	A	7·40	86·25	0·760	0·950	115·95	0·302	0·014	39·48
1648·4	345	A	10·04	83·88	0·910	0·940	113·62	0·332	0·008	43·39
2100·4	469	A	35·43	44·89	0·850	0·940	118·06	0·326	0·017	35·55
1294·1	265	B	6·02	88·34	0·930	0·910	133·23	0·431	0·011	38·96
1335·1	273	B	40·47	44·20	0·900	0·950	84·31	0·868	0·027	35·68
1530·0	315	B	12·49	76·72	0·820	0·950	94·31	0·435	0·012	37·05
1577·7	325	B	8·15	63·97	0·780	0·900	90·45	0·523	0·017	52·38
1670·1	353	B	8·49	83·62	0·910	0·950	126·43	0·265	0·008	46·68
1712·1	368	B	16·35	69·54	0·850	0·960	90·99	0·266	0·013	44·35
1936·3	428	B	0·19	81·45	0·930	0·930	129·40	0·491	0·023	33·67
1988·6	437	B	17·15	75·07	0·890	0·940	114·18	0·450	0·010	42·66
2152·5	484	B	5·42	88·76	0·710	0·900	87·30	0·241	0·005	40·71
2175·0	487	B	0·87	76·97	0·740	0·910	87·66	0·436	0·019	40·25
4166·3	996	B	13·32	79·02	0·731	0·900	86·08	0·260	0·003	36·22
4372·9	1063	B	6·89	86·26	0·722	0·890	81·64	0·463	0·008	32·64
4655·9	1129	B	14·26	70·36	0·800	0·915	85·60	0·318	0·012	34·92
1587·8	326	C	37·86	38·56	0·830	0·920	87·77	0·218	0·008	54·43
1813·8	397	C	31·94	50·21	0·880	0·880	91·92	0·201	0·012	40·43
1841·8	402	C	43·19	37·35	0·800	0·920	89·15	0·463	0·035	63·71
4422·7	1080	C	12·76	77·62	0·733	0·900	83·15	0·283	0·005	46·81

and a second set of correlation values were calculated.

Similar to Fe digestion tests, classification of the effect of organic matter on colour spectra was determined by obtaining colour spectra and FDS values from selected intervals in the sediment core. Approximately 0·5 g of sediment was used to create filter samples, using a similar technique to that found in Debret *et al.* (2006). Following reflectance measurements of the original smear slides, the sediment was treated with hydrogen peroxide (H_2O_2) to remove organic matter. Sediment samples were selected to encompass the range of total organic carbon (TOC) values found in the Lake El'gygytgyn sediments (0·5 to 3%; Melles *et al.*, 2012). Colour reflectance spectra produced from the two sets of analysis were then compared to determine the effect of organic matter on both visible and FDS spectra values.

RESULTS

Mineralogy

The major mineral phases for all 20 samples consisted of quartz, potassium and plagioclase feldspar minerals, and chlorite and illite. Quartz and clay minerals comprised the majority of the sediment. Interestingly, prior studies reported the presence of minerals such as vivianite (Asikainen *et al.*, 2007; Minyuk *et al.*, 2013) but, in the present study, vivianite was not detected by XRD analysis. Quartz ranged from 37·3 to 88·7%, while clay ranged from 0·2 to 43·19% and feldspars (K-spar and plagioclase) comprised a relatively minor component of the sediment, ranging from 0·21 to 9·9% and 3·6 to 25·9%, respectively (Table 1). Relative changes in the feldspar minerals do not co-vary with quartz or clay, while changes in quartz and clay abundances are inversely related. Samples with high clay percentages and low quartz abundances occur at 1335·1 cm, 1587·8 cm, 1813·8 cm, 1841·8 cm and 2100·4 cm depth. For the clay rich intervals, the samples at 1587·7 cm, 1813·8 cm and 1841·8 cm depth were found to correspond with the red laminated 'super interglacial' Facies C, as in Melles *et al.* (2012), while the samples at 1335·1 cm and 2100·4 cm corresponded to the massive, Facies B (Table 1).

In addition to mineral identification by XRD, SEM analysis was used to determine the presence of the iron-titanium oxide ilmenite, as well as to confirm the presence of quartz and feldspar

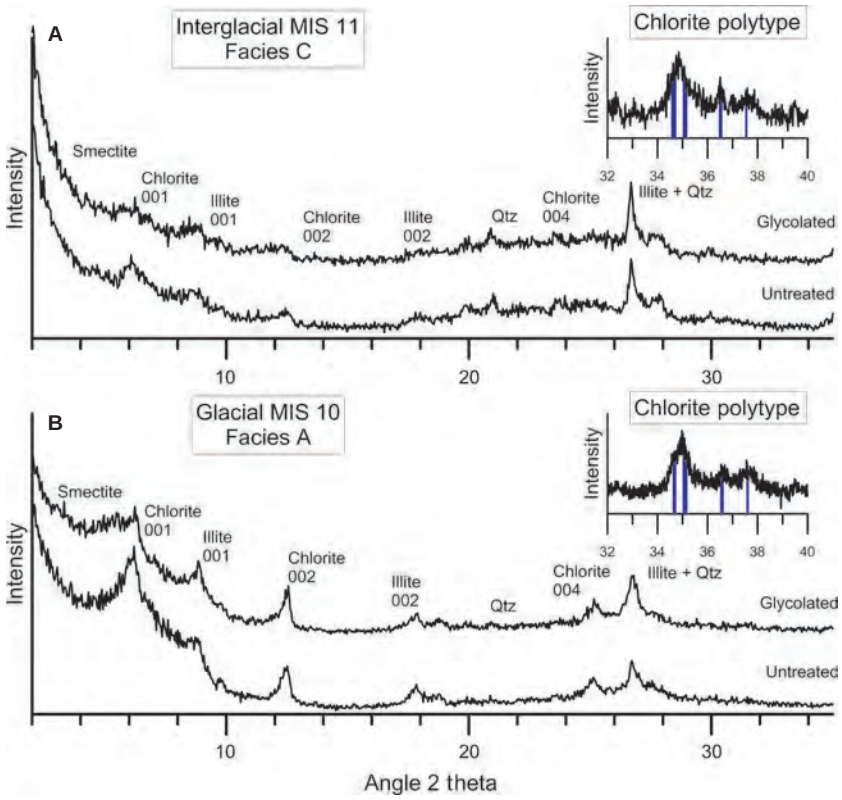

Fig. 6. Representative clay diffractograms for an interglacial and glacial sediment sample. Peaks used for identification are marked (d-spacings in angstroms). The insets demonstrate the chlorite IIb polytype peaks (blue) for both representative samples.

minerals. For interglacial samples, many quartz and feldspar grains were found to be coated with Fe-oxide stains. Additionally, investigations also demonstrated discrete veins of vivianite crystals, apparent only in thin sections prepared from Facies A sediments.

Three clay minerals in the <2 μm fraction were identified and quantified, with the largest component consisting of illite, followed by chlorite and smectite in terms of relative weight per cent (Fig. 6). While changes in the amount of total clay with respect to quartz occur on interglacial/glacial time scales, the relative percentages of clay minerals show a different trend. All three clay mineralogies do not fluctuate more than 10% above or below the average values measured in the core section, with an average of 13·8% smectite, 59·3% illite and 28·5% chlorite (Table 1).

The clay minerals in the <0·02 μm fraction included a slightly different assemblage of clay minerals in addition to illite, chlorite and smectite. The clay minerals kaolinite (0 to 11·4%), interlayered illite/smectite (90% illite: 0 to 25·88%) and trace amounts of chlorite/smectite were detected (Table 2). Analysis of clay polytypes suggests that the chlorite polytypes described for the Lake El'gygytgyn sediments are of the IIb variety (Fig. 6).

Grain-size data

Grain-size analyses revealed unique particle size differences between each of the three sediment facies. Overall, mean grain-size varied between 5·8 μm and 16·6 μm (mean = 8·8 μm), median sizes vary between 3·3 μm and 7·1 μm (mean = 4·1 μm) and mode sizes range between 2·3 μm and 13·6 μm (mean = 3·4 μm). The distribution of Facies A sediments is skewed towards finer grain-sizes (mean = 7·3 μm, median = 3·4 μm, mode = 2·6 μm), while Facies C contains more sediment falling into the coarser grain-sizes (mean = 12·4 μm, median = 4·2 μm, mode = 2·7 μm). Facies B sediments fall in between Facies A and C, with a mean size of 8·3 μm, median of 4·6 μm and mode of 3·8 μm. Variability in coarser (30 to 100 μm) sizes is most pronounced for the Facies C and some Facies B sediment samples (Fig. 7).

Raw colour and visible spectra data

The parameters of the CIE L*, a*, b* colour parameters indicate changes in brightness (L*), variations between green (−a*) and red (+a*), as well as blue (−b*) and yellow (+b*). For the L* parameter, values vary between 4·32% and

Table 2. Clay data measurements for the ultra fine (<0·02 μm) clay fraction, as well as clay measurement data from deeper intervals from the Lake El'gygytgyn sediment core. I/S 90 refers to interlayered 90% illite with 10% smectite.

Depth (cm)	Age (ka)	Facies	Smectite (%)	Illite (%)	Chlorite (%)	Kaolinite (%)	I/S (90) (%)	Expandable totals (%)
1379·5	265	A	9·22	45·82	27·30	6·52	11·14	11·14
1648·4	273	A	12·11	49·77	17·95	6·31	13·87	13·87
2100·4	283	A	11·14	48·97	19·01	7·63	13·25	13·25
1294·1	315	B	3·83	68·60	13·47	5·05	9·05	9·05
1335·1	325	B	9·16	53·09	16·86	7·34	13·56	13·56
1530·0	326	B	4·01	47·13	24·38	7·35	17·13	17·13
1577·7	345	B	13·45	58·23	14·94	4·36	9·03	9·03
1670·1	353	B	6·99	45·84	17·70	3·59	25·88	25·88
1712·1	368	B	7·00	47·34	20·36	9·78	15·52	15·52
1936·3	397	B	5·93	53·17	12·81	3·34	24·74	24·74
1988·6	402	B	8·73	51·94	17·37	7·79	14·17	14·17
2152·5	428	B	7·67	58·54	15·54	4·80	13·45	13·45
2172·5	437	B	10·73	50·43	17·96	7·26	13·62	13·62
1587·8	469	C	8·48	55·03	14·79	5·62	16·09	16·09
1813·8	484	C	8·35	66·55	13·70	11·40	0·00	0·00
1841·8	487	C	11·08	70·91	18·01	0·00	0·00	0·00

65·77% reflectance, with an average of 42·51%. The a* parameter values vary between −6·18% and 2·81% with an average value of −1·41%, while the b* parameter values range from −0·97 to 18·94% with an average reflectance of 5·60%, while the calculated hue value [Hue = atan2 (a*, b*)] has values which vary between 77·63 and 150·2 with an average hue of 107·59 (Fig. 2; Table 1).

All of the colour parameters, except for the L* parameter, suggest changes in sediment colour through time. Changes in the L* parameter represent changes in the brightness of the sediment, which stays relatively stable at values of *ca* 42% reflectance. Colour values in the red value range (lower values; red = 0°, 360°) at depths of *ca* 1550 to 1600 cm and 1800 to 1900 cm, correspond to the red laminated facies (Facies C; Melles *et al.*, 2012; Supplementary Materials) observed in the Lake El'gygytgyn core. At depths of 1300 to 1350 cm, 1600 to 1700 cm and 1950 to 2100 cm, *ca* 1550 to 1600 cm and 1800 to 1900 cm, the hue values are significantly higher (Fig. 6), corresponding to Facies A with green hue values (green = 180°). In between sections of red (Facies C) and green (Facies A) sediments, are the Facies B sediments, which vary in respec-

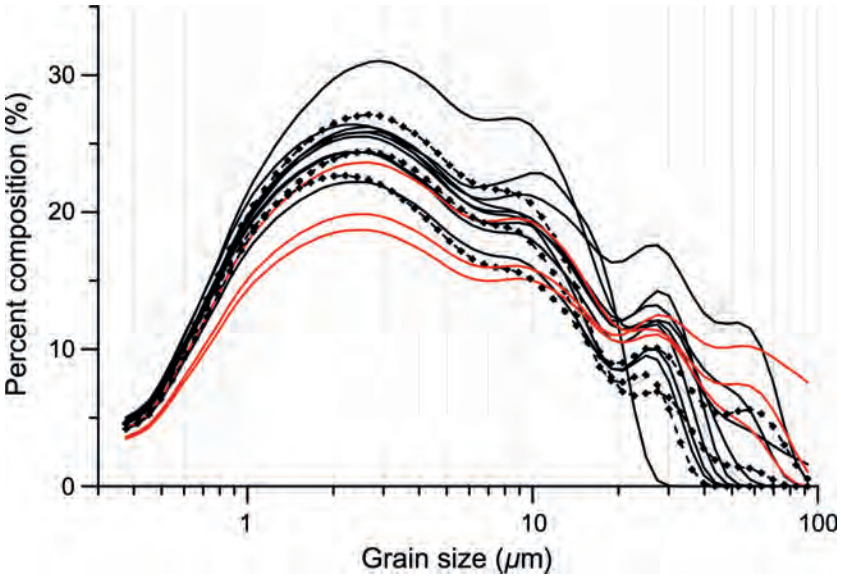

Fig. 7. Grain-size distributions for selected samples, coloured by facies: Black, solid lines = Facies B; Red = Facies C; and dashed line with diamond symbols = Facies A.

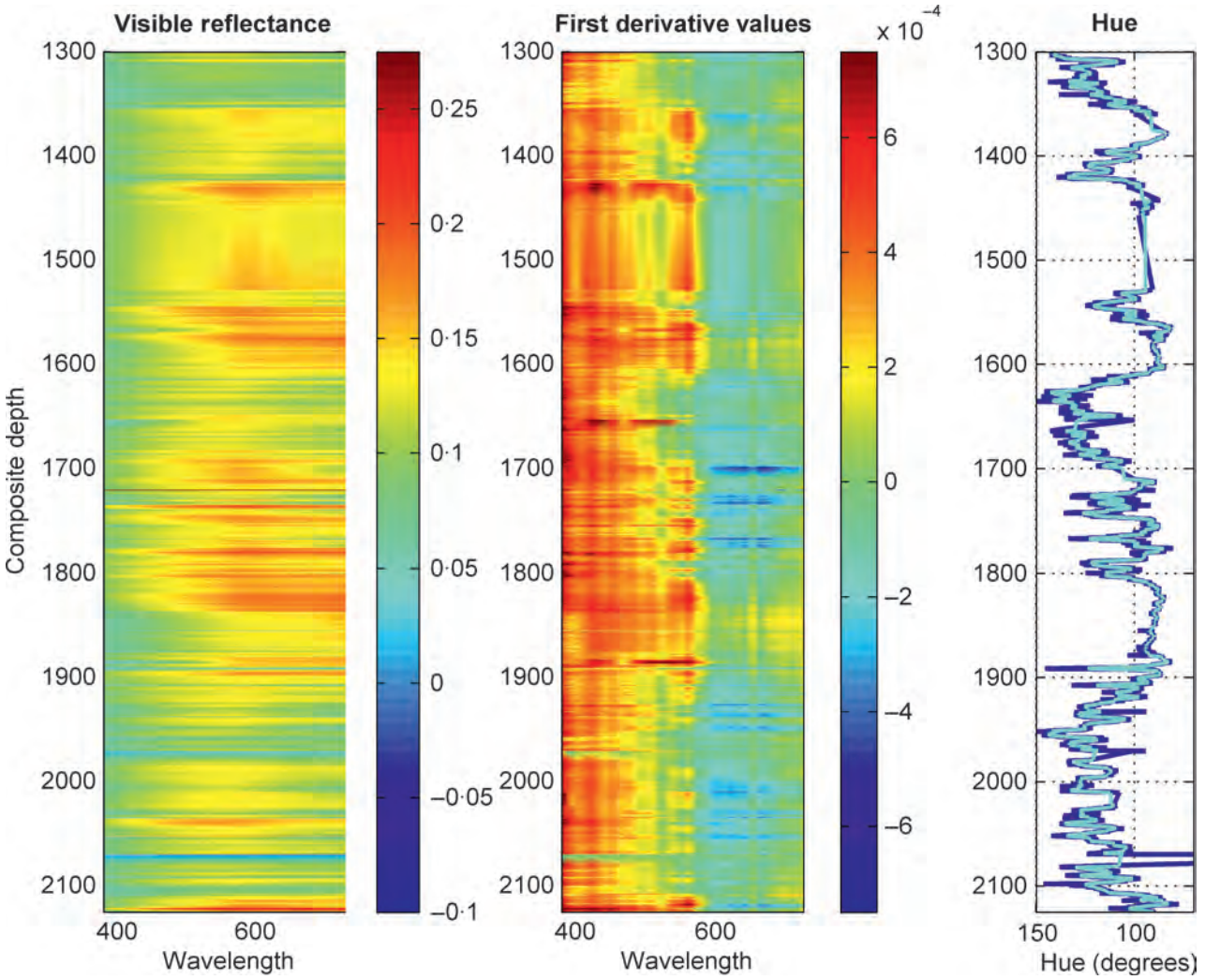

Fig. 8. Surface plots coloured to represent the variability of both VIS (left) and FDS (middle). Both the VIS and FDS can be linked to the hue colour parameter (right), with higher VIS values in the red (600 to 700 nm) area correlated with lower (red) hue values. Note the variability in the FDS values in the 550 nm range, because studies link variations in the 550 nm wavelength to iron oxide content (Deaton & Balsam, 1991; Debret *et al.*, 2011).

tive hue vales between red and green values. The a* and b* parameters follow similar trends as hue, although changes are more pronounced in the a* values with depth than with the corresponding b* values.

The inherent differences in hue values are reflected in varying VIS plots, because the structure of each spectrum for discrete depths downcore varies significantly, most notably in the *ca* 550 to 730 nm range. The red, interglacial facies (Facies C) have a distinct structure with reflectance values highest in the *ca* 600 to 700 nm band range, and a generally positive slope indicative of a positive relation with increasing band length (Figs 5 and 8). On the other hand, the green, glacial facies (Facies A) also has a unique signature, characterized by a peak centred on the 550 nm band (Figs 5 and 8).

First derivative spectra values

First derivative spectra (FDS) values fluctuate most dramatically in the 550 nm portion of the spectrum, as well as from 600 to 700 nm. For the 550 nm spectral band, the most notable FDS changes occur at *ca* 1550 to 1600 cm depth and *ca* 1800 to 1900 cm depth, as well as notable higher frequency fluctuations between *ca* 1700 cm and 1800 cm depth. In the 600 to 700 nm range, changes in FDS values are not as dramatic as in the 550 nm band, but nonetheless fluctuate with depth. The highest values are

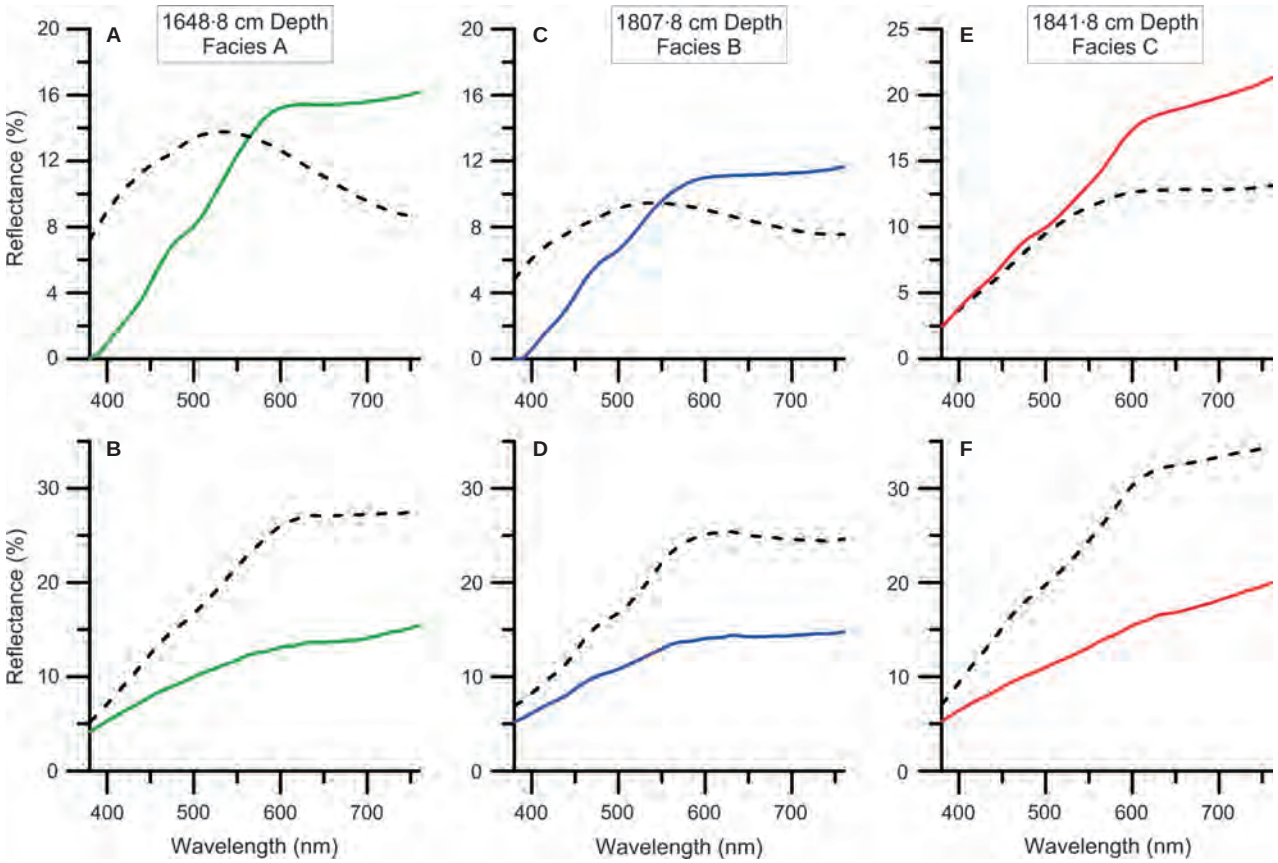

Fig. 9. Top plots demonstrate the measured colour VIS continuums before (coloured plots) and after (dashed black) iron digestion tests for representative facies samples. Note how the spectra shifts to centring on the green (*ca* 500 nm) wavelengths. Bottom plots show before (coloured plots) and after (black dashed) TOC removal by H_2O_2 treatment. Notable increases in reflectance are observed post-removal of organic content.

found in the intervals at *ca* 1550 to 1600 cm and 1700 to 1800 cm. The lowest values occur during the *ca* 1700 to 1800 cm depth intervals, with low values from *ca* 1950 cm, and from 2000 to 2050 cm composite depth (Fig. 8).

The range of r values from the 20 sediment samples from correlations between measured and reconstructed FDS values is from 0·71 to 0·93, with the low correlation values found during the interglacial sediments (Facies B and C) and the highest values from the glacial (Facies A) sediments (Table 1; Fig. 5).

Calibration results – Total organic carbon and Fe-oxide analysis

Investigations into the effect of organic matter on the sediment reflectance parameters indicate significant changes between relatively organic rich sediments and sediments lacking in organic matter. The sediment sample with the lowest TOC percentage (0·29%) experienced the least change in the VIS spectrum, with a slight (1·8% reflectance) brightening of the sediments when organic matter was destroyed. In samples with higher values of TOC (0·9% and higher), the VIS continuums show a greater brightening of the sediments, with average reflectance differences varying between 7·1% and 11·1% reflectance. Changes in the FDS continuums were also noted, with removal of organic material resulting in the accentuation of multiple peaks in the treated samples when compared with the original, organic rich sediment samples (Fig. 9). Similar to the VIS measurements, minimal changes with the 0·29% TOC sample were noticed, while larger peak accentuations were observed for the TOC rich (0·9 to 2%) sediments (Fig. 9).

Iron digestion sensitivity tests reveal for all facies a shift in the colour spectrum towards the green portions (400 to 500 nm) of the visible spectrum (Fig. 10). Colour measurements also demonstrate improved correlation coefficients (r values; Table 1) following the iron digestion

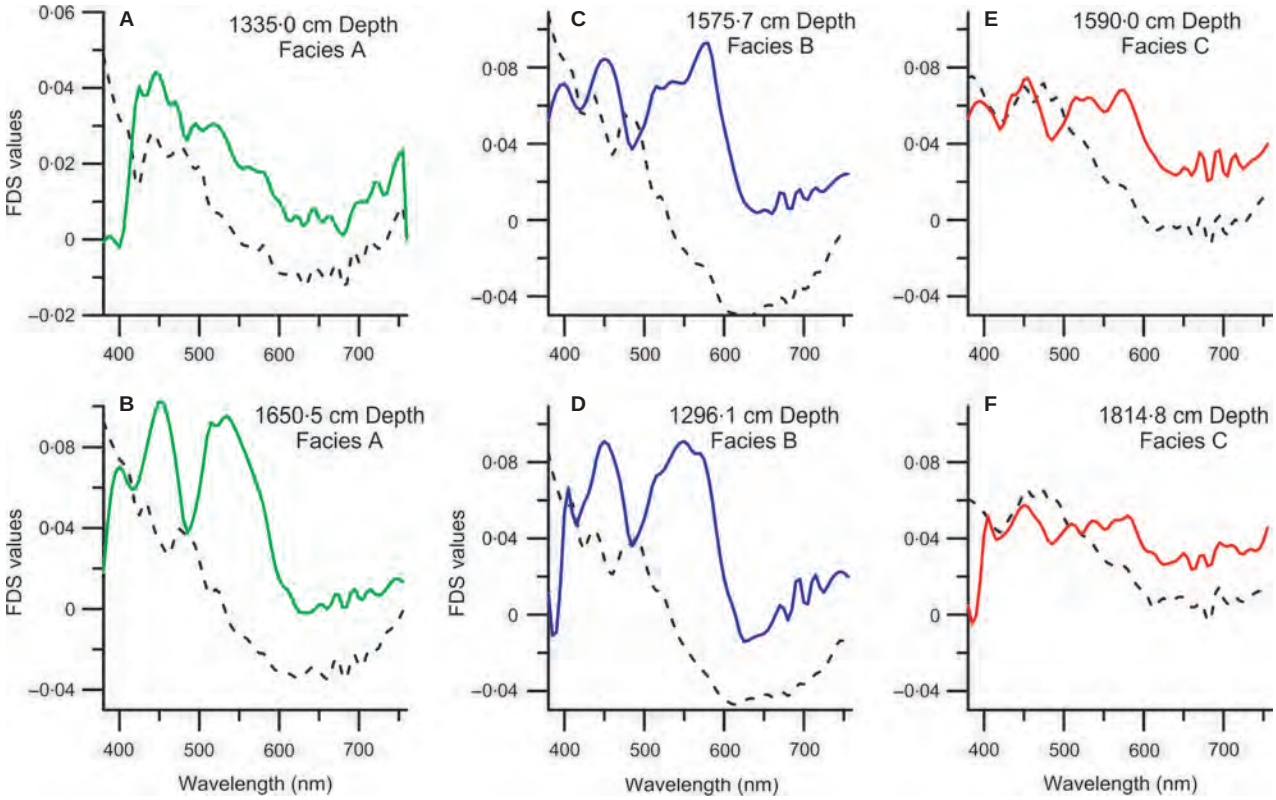

Fig. 10. Calculated FDS values for iron digestion experiment for representative facies, before (coloured) and after (dashed black) iron oxide removal. Note how peaks at 450 nm and 550 nm disappear post-removal of iron oxides, similar to results from prior studies of iron oxides and sediment colour (Deaton & Balsam, 1991; Debret *et al.*, 2011).

techniques, with a smaller range of r values (0·88 to 0·96). Additionally, measured concentrations of digested Fe and Mn oxides range from 0·21 to 0·90% by weight for Fe-oxides, and from 0·005 to 0·027% by weight for Mn oxides. Within facies, the mean concentrations of Fe for Facies A are 0·32% (standard deviation = 0·015%). For Facies B and C the mean concentrations measured were 0·44% (standard deviation = 0·18%) and 0·29% (standard deviation = 0·14%), respectively (Table 1).

DISCUSSION

The overall colour signal demonstrates a remarkable correspondence to climate fluctuations, with clear colour differences between sediments deposited during cold periods versus those deposited during warmer conditions. These colour variations are not driven solely by large-scale interglacial – glacial changes, although comparison with climate proxies records, such as global benthic foraminifera stacks, suggests that these changes dominate the record (Lisiecki & Raymo, 2005; Fig. 2). Notably, the hue parameter demonstrates variability on more rapid time scales than the changes between full interglacial and full glacial conditions (Fig. 2), suggesting that the hue parameter is recording a lake system that is sensitive to higher frequency shifts in past climate and environmental conditions.

Mineralogy

Analysis of the bulk mineralogy reveals shifts in relative inputs of the major minerals to the lake, because these shifts occur in conjunction with changes between interglacial and glacial conditions. Relative changes in the amounts of quartz and the input of clay minerals are the most notable. During glacial periods, quartz dominates the input to the lake, coupled with low amounts of clay minerals. Interglacial intervals, on the other hand, show less quartz and more clay material deposited in the lake (Table 1). Higher inputs of

clay are also not restricted to the defined interglacials MIS 9 and MIS 11; rather, high clay input in samples corresponding with red hues outside of Facies B suggests fluctuations in catchment processes. Interestingly, when compared with other available biological proxies, such as biogenic silica, pollen counts (Melles *et al.*, 2012; Vogel *et al.*, 2013) or biomarkers (D'anjou *et al.*, 2013) from Lake El'gygytgyn during this time period, proxies for productivity fail to capture the variability demonstrated by the hue and mineral abundances (Fig. 2). This finding suggests that the hue parameter may capture variability of the physical and chemical catchment processes, and that catchment processes are sensitive to additional environmental changes not recorded in some other proxy records.

Unlike the glacial/interglacial variability of the bulk mineralogy, the relative amounts of the clay minerals chlorite, illite and smectite, remain relatively fixed throughout the MIS 8 to 12 interval. Clay analyses show increases in the amount of clay but not a specific clay mineral, suggesting a catchment driven by mechanical weathering processes as opposed to the authigenic formation of clays in the catchment (Table 1). Analysis of chlorite polytypes supports mechanical weathering processes, because the IIb polytype was the only polytype identified for all sediment facies (Fig. 6). The IIb polytype, which forms in metamorphic rocks (Hayes, 1970), demonstrates that the detrital origin of the chlorite clay minerals, such as authigenic chlorites would probably be of the Ia variety formed at lower temperatures (Walker, 1993). Thus, increases in the total amount of clay imply a wetter climate, with higher precipitation increasing the physical transport of clay material into the lake.

Colour sensitivity

Although mechanical weathering encapsulates the majority of weathering around the lake catchment, the variability in the colour spectra not explained by XRD and reference mineral spectra implies additional sediment components and possible chemical weathering processes (Fig. 5). Iron oxide minerals, especially the oxide mineral hematite, are known to stain sediments. Iron digestion tests demonstrate the presence of iron oxides in the sediments, and also the relative amount of colour signals produced by iron oxide staining (Fig. 10). For Facies B sediments, removal of iron oxides results in green colour signals resembling sediments from the glacial Facies A. Calculated correlation values for all facies improve significantly when FDS continuums from mineral abundance reconstructions are compared with those measured following the iron digestion (Table 1; Fig. 5), suggesting that bulk mineralogy contributes a significant background colour signal. When increases in the amount of iron oxide formation in the catchment occur, these oxides contribute a red colour signal in addition to the background mineral colours, which ultimately stain the sediments red and are reflected in the low hue values observed during both Facies B and C.

When the iron digestion tests are applied to Facies C, however, notable reflections in the red portion of the spectrum still exist, suggesting that the red hues from Facies C are driven by both the iron oxide and TOC signals. Results from colour sensitivity tests elucidate the relative effects of organic matter and iron oxide minerals on colour spectra. Organic matter inputs, which can be approximated by TOC, brighten sediment colour when removed, especially in the red (600 to 700 nm) wavelengths of the visible colour spectrum, and are also reflected in the FDS continuums (Figs 9 and 10). Low TOC values (<0·5%) correspond to glacial sediments and Facies A, and these sediments exhibited the smallest measured colour change from TOC sensitivity tests. In sediments where TOC percentages are highest (up to 2%) corresponding to the 'super interglacial' stages (Melles *et al.*, 2012), the most sediment brightening with the removal of organic content occurs while also contributing a colour signal in the red portions of the visible spectrum. Previous colour investigations have shown that high TOC content drives sediment colour changes in the visible spectrum (Debret *et al.*, 2011), and various pigments from chlorophylls and carotenoid compounds also have visible reflections in the red portion of the visible spectrum (Rein & Sirocko, 2002; Wolfe *et al.*, 2006). These results elucidate key differences between the red sediments between Facies C and Facies B; that is, the red hues in Facies B are derived from iron oxides, while the red hues in Facies C are both iron oxide and organic matter driven. While hue values may suggest that similar processes occur during the deposition of both Facies C and B, analysis of the FDS and visible colour spectra reveal the weathering differences that define Facies C as 'super interglacial' periods.

Iron digestion solution analysis

Coupled with analysis of the colour signal from iron oxide removal, analysis of the Fe and Mn ions present in the digested solution supports mechanical weathering processes sourced from the lake catchment. The concentrations measured yield similar, low concentrations of Fe for Facies A sediments, while the measurements for Facies B and C exhibit a wide range of concentrations and cannot be differentiated from one another. Both iron oxides and manganese oxides are ubiquitous in soils (Jackson, 1969; Post, 1999), and the erosion, transport and deposition of these oxides into lake sediments drive the hue colour parameter. For Facies A, the low measured Fe and Mn content corresponds with the greenish/grey sediment colours, supporting the colour analysis, which points to a lack of available material for oxidation in the catchment during drier periods.

In contrast, the Fe and Mn concentrations for Facies B and C sediments demonstrate higher variability than the Facies A sediments. For some Facies B and C sediments, high amounts of clay and red hue values are associated with relatively high abundances of iron oxide material, while other samples demonstrate low measured iron oxide abundances despite red hue values. For the samples with red hues and high concentrations of iron oxides, the red sediment colour can be directly linked to iron oxide staining, and an increase in physical weathering and transport. The processes affecting samples with lower oxide abundances but with red hues, however, can be linked with periods of high TOC in some cases (three of the Facies C samples, and Facies B at 1335·1 cm depth), indicative of higher rates of organic deposition and/or preservation. As discussed above, organic matter contributes a red colour signal, and for these sediment samples, particularly the Facies C sediments, the red hues are generated from a mix of iron oxides and organic inputs.

Samples with both low iron oxide abundances and low TOC suggest additional processes; interpretations by Melles *et al.* (2012) suggest periods of oxygen depletion within the water column during the deposition of both Facies A and Facies C. Analysis of the Mn and Fe abundances based on the digestion solution measurements and the calculated Mn/Fe ratio, however, do not support this hypothesis, because none of the three facies demonstrates consistent ratio values. Instead, the measured abundances and the calculated Mn/Fe ratio imply variability in the preservation of both iron and manganese oxides in the sediment, and that suboxic conditions may have persisted at different times and to varying degrees within the water column.

Interglacial/glacial period variability

The suite of analyses examined in this study provides insights into relations between past environmental conditions and sediment colour. Glacial period sediments (Facies A) are characterized by a unique colour signature, with higher hue values indicative of a green/grey colour. The overall green colour of the glacial sediments reflects a largely detrital mineral signal, with total clay, TOC values and digested iron oxide concentrations all low during these times. Such a colour signal dominated by mineral input suggests that processes such as chemical weathering were almost non-existent during glacial intervals, which is indicative of a cold and dry lake catchment. Mechanical weathering processes typical of cold environments were probably active but still limited, as demonstrated by the lack of variations in clay minerals as well as chlorite polytypes and the Fe and Mn digestion solution data. Drier conditions limited the production of physically weathered material and Fe-bearing silicate minerals, and therefore limited iron oxide input into the lake, colouring the sediments the distinctive green/grey hue.

The red colour measured in many Facies B samples corresponds with the presence of Fe-oxides/hydroxides during wetter intervals. The relation between Fe-oxides such as hematite is well-known in both soils (Torrent *et al.*, 1983) and in sediments (Deaton & Balsam, 1991), and it must be noted that small amounts of iron oxide abundances (<0·5%) can drive sediment colour changes (Deaton & Balsam, 1991). For this lake system, the colour signals represented by iron oxides are overprinted on the background mineralogical colour signals, represented in the green Facies A. Thus, the presence of increased Fe-oxides implies a slightly greater degree of chemical weathering around the lake catchment, because enhanced physical erosion as a result of wetter environmental conditions would increase the amounts of Fe-bearing silicates available for oxidation, and their ultimate deposition in the lake sediments. Interestingly,

periods of enhanced iron oxide deposition do not necessary occur in conjunction with interglacial periods, suggesting wet interval cycles out of phase with only interglacial/glacial variability.

Facies C sediments, while also demonstrating red hue values, do not share the same sedimentary components as their Facies B counterparts. Because the colour signal from organic inputs also contributes a red colour, the Facies C sediments can be linked to climate conditions that were both warm and wet, as demonstrated from VIS and FDS continuums. These facies occur in MIS 9 and MIS 11 and are interpreted as 'super interglacial' intervals (Melles *et al.*, 2012), an interpretation supported by previous pollen reconstructions (Lozhkin *et al.*, 2013) and biomarker data (D'anjou *et al.*, 2013). These differences then set the red Facies C sediments apart from the red Facies B sediments in terms of lake processes, and allow for palaeoclimate interpretations of the hue record.

The hue record overall can be interpreted to represent the gradational changes of the lake from relatively dry to relatively wet conditions. Enhanced moisture around the lake during these periods produced more material for chemical weathering, which is represented by red iron oxide staining ultimately overprinted on a glacial background mineral colour signal. It must be noted, however, that although similar red hues for Facies B and C exist, the 'super interglacial' periods during MIS 9, 11 and 31 represent climatic intervals that were relatively warm and wet, while red Facies B sediments reflect only enhanced moisture. Based on this assessment, interesting wet periods stand out in the hue record, most notably during glacial periods MIS 6, 8, 10 and 16 (Fig. 2). While some suggested moisture intervals, like those in MIS 8, can be linked to global climate shifts apparent in global records, enhanced moisture events such as those in MIS 10 and MIS 12 do not appear at a hemispheric scale. Notably, a cold yet moist MIS 6 in the Mediterranean Sea region (Bard *et al.*, 2002), as well as African monsoon enhancement, have been recorded (Tisserand *et al.*, 2009) and may be seemingly recorded in the Lake El'gygytgyn hue record. These colour measurements from the entire length of the ICDP 5011-1 core can then potentially provide continuous, climatic information for glacial/interglacial periods not yet understood in the terrestrial Arctic setting.

CONCLUSIONS

This study demonstrates overall the strong relation between sediment mineralogy and other sedimentary components on the ultimate sediment colour, measured by high-resolution core scans. The use of sediment colour, and specifically the hue colour parameter, can then be used as a proxy for processes occurring within the Lake El'gygytgyn processes. The colour signal is dominated by clastic inputs, demonstrated by measuring bulk mineralogy and pairing these data with colour spectra reconstructions. Colour sensitivity tests show the importance of both organic material and iron oxide minerals on sediment colour as well, with these minor sedimentary components overprinting their colour signal over those of the background mineral content. The fluctuating concentrations of various sedimentary components are driven by the dominant mechanical erosion and physical transport of sediment into the lake basin, with physical processes demonstrated by clay mineral analysis. Interpretation of the hue colour proxy suggests an intensification of physical weathering processes during wetter periods, driving more clastic input as well as increasing iron oxide formation which, in turn, drives the observed colour changes from green sediment during cold, dry glacial intervals to red sediments during warmer and wetter interglacial intervals. Overall, the validation of the hue colour record provides insights into climate fluctuations for the MIS 8 to MIS 12 interval, and the techniques discussed in this study can be used to calibrate and analyse future sediment records where high-resolution core scanning techniques are applicable.

ACKNOWLEDGEMENTS

Funding for this research was provided by the International Continental Scientific Drilling Program (ICDP), the US National Science Foundation (NSF), the German Federal Ministry of Education and Research (BMBF), Alfred Wegener Institute (AWI) and GeoForschungsZentrum Potsdam (GFZ), the Russian Academy of Sciences Far East Branch (RAS FEB), the Russian Foundation for Basic Research (RFBR), and the Austrian Federal Ministry of Science and Research (BMWF). The Russian GLAD 800 drilling system was developed and operated by DOSECC Inc., the downhole logging was

performed by the ICDP-OSG, and LacCore, at the University of Minnesota, handled core curation. Raw pollen data were provided by Anatoly Lozhkin, NEISRI, and Patricia Anderson, University of Washington. We especially acknowledge NSF support for grant # EAR-0602471.

REFERENCES

Asikainen, C.A., **Francus, P.** and **Brigham-Grette, J.** (2007) Sedimentology, clay mineralogy and grain-size indicators of 65 ka of climate change from El'gygytgyn Crater Lake, Northeastern Siberia. *J. Paleolimnol.*, **37**, 105–122.

Balsam, W.L. and **Beeson, J.P.** (2003) Sea-floor sediment distribution in the Gulf of Mexico. *Deep Sea Res.*, **1**, 1421–1444.

Balsam, W.L., **Deaton, B.C.** and **Damuth, J.E.** (1998) The effects of water content on diffuse spectrophotometry studies of deep-sea sediment cores. *Mar. Geol.*, **149**, 177–189.

Bard, E., **Delaygue, G.**, **Rostek, F.**, **Antonioli, F.**, **Silenzi, S.** and **Schrag, D.P.** (2002) Hydrological conditions over the western Mediterranean basin during the deposition of cold Sapropel 6 (ca. 175 kyr BP). *Earth Planet. Sci. Lett.*, **202**, 481–494.

Barranco, F.T., **Balsam, W.L.** and **Deaton, B.C.** (1989) Quantitative reassessement of brick red lutites – evidence from réflectance spectrophotometry. *Mar. Geol.*, **89**, 299–314.

Bayliss, P. (1986) Quantitative analysis of sedimentary minerals by powder X-ray diffraction. *Powder Diffract.*, **1**, 37–39.

Belyi, V. and **Belaya, B.** (1998) *Late Stage of the Okhotsk-Chukchi Volcanogenic Belt Development (Upstream of the Enmyvaam River)*. NEISRI FEB RAS, Magadan, 108 pp.

Belyi, V. and **Raikevich, M.I.** (1994) *The El'gygytgyn Lake Basin (Geological Structure, Morphostructure, Impactites, Problems of Investigation and Preservation of Nature)*. NEISRI FEB RAS, Magadan, 27 pp.

Brown, B.E. and **Bailey, S.W.** (1963) Chlorite Polytypism: II. Crystal Structure of a One-layer Cr-Chlorite. *Am. Mineral.*, **28**, 42–61.

Brown, G. and **Brindley, G.W.** (1980) X-ray diffraction procedures for clay mineral identification. In: *Crystal Structures of Clay Minerals and their X-ray Identification* (Eds G.W. Brindley and G. Brown), *Mineral. Soc. London*, **London**, 305–329.

Clark, R.N., **Swayze, G.A.**, **Wise, R.**, **Livo, E.**, **Hoefen, T.**, **Kokaly, R.** and **Sutley, S.J.** (2007) USGS digital spectral library splib06a. *US Geol. Surv. Digital Data Ser.*, **231**. Available at: http://speclab.cr.usgs.gov/spectral.lib06/ds231/index.html#SMSE.

D'Anjou, R.M., **Wei, J.H.**, **Castañeda, I.S.**, **Brigham-Grette, J.**, **Petsch, S.T.** and **Finkelstein, D.B.** (2013) High-latitude environmental change during MIS 9 & 11: biogeochemical evidence from Lake El'gygytgyn, Far East Russia. *Clim. Past*, **9**, 567–581.

Deaton, B. and **Balsam, W.** (1991) Visible spectroscopy – a rapid method for determining hematite and goethite concentration in geological materials. *J. Sed. Petrol.*, **61**, 628–632.

Debret, M., **Desmet, M.**, **Balsam, W.**, **Copard, Y.**, **Francus, P.** and **Laj, C.** (2006) Spectrophotometer analysis of Holocene sediments from an anoxic fjord: Saanich Inlet, British Columbia, Canada. *Mar. Geol.*, **229**, 15–28.

Debret, M., **Sebag, D.**, **Desmet, N.**, **Balsam, W.**, **Copard, Y.**, **Mourier, B.**, **Susperrigui, A.-S.**, **Arnaud, F.**, **Bentaleb, I.**, **Chapron, E.**, **Lallier-Verges, E.** and **Winiarski, T.** (2011) Spectrocolorimetric interpretation of sedimentary dynamics: the new "Q7/4 diagram. *Earth Sci. Rev.*, **109**, 1–19.

Deplazes, G., **Lüchge, A.**, **Peterson, L.C.**, **Timmermann, A.**, **Hamann, Y.**, **Hughen, K.A.**, **Röhl, U.**, **Laj, C.**, **Cane, M.A.**, **Sigman, D.M.** and **Haug, G.H.** (2013) Links between tropical rainfall and North Atlantic climate during the last glacial period. *Nat. Geosci.*, **6**, 213–217.

EPICA Community Members (2004) Eight glacial cycles from an Antarctic ice core. *Nature*, **429**, 623–628.

Gibbs, R.J. (1977) Clay mineral segregation in the marine environment. *J. Sed. Petrol.*, **47**, 237–243.

Hayes, J.B. (1970) Polytypism of chlorite in sedimentary rocks. *Clay Clay Mineral.*, **18**, 285–306.

Helmke, J.P., **Shulz, M.** and **Bauch, H.A.** (2002) Sediment Color Record from the Northeast Atlantic Reveals Patterns of Millennial-Scale Climate Variability during the past 500,000 years. *Quatern. Res.*, **57**, 49–57.

Hoffman, J. (1976) *Regional Metamorphism and K-Ar Dating of Clay Minerals in Cretaceous Sediments of the Disturbed Belt of Montana*. PhD thesis, Case Western Reserve University, Cleveland, OH, 266 pp.

Jackson, M.L. (1969) *Soil Chemical Analysis: Advanced Course*, pp. 44–52. Parallel Press, Madison, WI.

Ji, J., **Shen, J.**, **Balsam, W.**, **Chen, J.**, **Liu, L.** and **Liu, X.** (2005) Asian monsoon oscillations in the northeastern Qinghai-Tibet Plateau since the late glacial as interpreted from visible reflectance of Qinghai Lake sediments. *Earth Planet. Sci. Lett.*, **233**, 61–70.

Lawrence, K.T., **Herbert, T.D.**, **Brown, C.M.**, **Raymo, M.E.** and **Haywood, A.M.** (2009) High amplitude variations in North Atlantic sea surface temperature during the early pliocene warm period. *Paleoceanography*, **24**, PA2218. doi: 10/1029/2008PA001669.

Layer, P.W. (2000) Argon-40/argon-39 age of the El'gygytgyn impact event, Chukotka, Russia. *Meteor. Planet. Sci.*, **35**, 591–599.

Lisiecki, L.E. and **Raymo, M.** (2005) A Pliocene-Pleistocene stack of 57 globally distributed benthic δ18O records. *Paleoceanography*, **20**, PA1003. doi: 10.1029/2004pa001071.

Loutre, M.F. and **Berger, A.** (2002) Marine Isotope Stage 11 as an analogue for the present interglacial. *Global Planet. Change*, **36**, 209–217.

Lozhkin, A.V., **Anderson, P.M.M.**, **Matrosova, T.V.**, and **Minyuk, P.S.** (2007) The pollen record from El'gygytgyn Lake: implications for vegetation and climate histories of norther Chukotka since the late middle Pleistocene. *J. Paleolimnol.*, **37**, 135–153.

Lozhkin, A.V. and **Anderson, P.M.** (2013) Vegetation responses to interglacial warming in the Arctic: examples from Lake El'gygytgyn. *Far East Russian Arctic. Clim. Past*, **9**, 1211–1219.

Melles, M., **Brigham-Grette, J.**, **Minyuk, P.S.**, **Nowaczyk, N.R.**, **Wennrich, V.**, **DeConto, R.M.**, **Anderson, P.M.**, **Andreev, A.A.**, **Coletti, A.**, **Cook, T.L.**, **Haltia-Hovi, E.**, **Kukkonen, M.**, **Lozhkin, A.V.**, **Rosen, P.**, **Tarasov, P.**, **Vogel, H.** and **Wagner, B.** (2012) 2.8 million years of arctic

climate change from lake El'gygytgyn, NE Russia. *Science*, **337**, 315–320.

Minyuk, P.S., **Borkhodoev, V.Y.** and **Wennrich, V.** (2013) Inorganic data from El'gygytgyn Lake sediments: stages 6–11. *Clim. Past*, **9**, 343–433.

Mix, A.C., **Rugh, W.**, **Pisias, N.G.** and **Viers, S.** (1992) Leg 138 Shipboard Sedimentologists, and the Leg 138 scientific party: color reflectance spectroscopy: a tool for rapid characterization of deep-sea sediments. *Proc. ODP Sci. Results*, **138**, 67–77.

Moore, D.M. and **Reynolds, R.C., Jr.** (1997) *X-Ray Diffraction and the Identification and Analysis of Clay Minerals*, 2nd edn. Oxford University Press, New York.

Moy, C.M., **Seltzer, G.O.**, **Rodbell, D.T.** and **Anderson, D.M.** (2002) Variability of El Niño/Southern Oscillation activity at millennial timescales during the Holocene epoch. *Nature*, **420**, 162–165.

Nolan, M. (2013) Analysis of local AWS and NCEP/NCAR reanalysis data at Lake El' gygytgyn, and its implications for maintaining multi-year lake-ice covers. *Clim. Past Discuss.*, **8**, 1443–1483.

Nolan, M. and **Brigham-Grette, J.** (2007) Basic hydrology, limnology, and meteorology of modern Lake El'gygytgyn, Siberia. *J. Paleolimnol.*, **37**, 17–35.

Nowaczyk, N.R., **Haltia-Hovi, E.M.**, **Ulbricth, D.**, **Wennrich, V.**, **Kukkonen, M.**, **Rosén, P.**, **Vogel, H.**, **Meyer-Jacob, C.**, **Andreev, A.**, **Lozhkinm, A.V.** and El'gygytgyn Scientific Party (2013) Chronology of Lake El'gygytgyn sediments. *Clim. Past*, **9**, 2413–2432.

Ortiz, J.D., **Polyak, L.**, **Grebmeier, J.M.**, **Darby, D.**, **Eberl, D.D.**, **Naide, S.** and **Nof, D.** (2009) Provenance of Holocene sediment in the Chukchi-Alaskan margin based on combined diffuse spectral reflectance and quantitative X-Ray Diffraction analyses. *Global Planet. Change*, **68**, 73–84.

Post, J.E. (1999) Manganese oxide minerals: crystal structures and economic and environmental significance. *Proc. Natl Acad. Sci.*, **96**, 3447–3454.

Prokopenko, A.A., **Bezrukova, E.V.**, **Khursevich, G.K.**, **Solotchina, E.P.**, **Kuzmin, M.I.** and **Tarasov, P.E.** (2010) Climate in continental interior Asia during the longest interglacial of the past 500 000 years: the new MIS 11 record from Lake Baikal Se Siberia. *Clim. Past*, **6**, 31–48.

Raymo, M.E. and **Mitrovica, J.X.** (2012) Collapse of polar ice sheets during the stage 11 interglacial. *Nature*, **483**, 453–456.

Rein, B. and **Sirocko, F.** (2002) In-Situ reflectance spectroscopy – analyzing techniques for high-resolution pigment logging in sediment cores. *Int. J. Earth Sci.*, **91**, 950–954.

Reynolds, R.C. (1980) Interstratified clay minerals. In: *Crystal Structures of Clay Minerals and their X-ray Identification* (Eds G.W. Brindley and G. Brown), *Mineral. Soc. London*, **5**, 249–303.

Reynolds, R.C. (1985) *NEWMOD – Program for the Calculation of the One-Dimensional X-Ray Diffraction Patterns of Mixed-Layer Clays*. Reynolds, R.C., Hanover, NH.

Reynolds, R.C. (1989) Principles and techniques of quantitative analysis of clay minerals by X-ray powder diffraction. In: *Quantitative Mineral Analyses of Clays* (Eds D.R. Pevear and F.A. Mumpton), pp. 4–36. Clay Minerals Society, Evergreen, CO.

Schwamborn, G., **Fedorov, G.**, **Schirrmeister, L.**, **Meyer, H.** and **Hubberten, H.-W.** (2008) Periglacial sediment variations controlled by lake level rise and Late Quaternary climate at El'gygytgyn Crater Lake, Arctic Siberia. *Boreas*, **37**, 55–65.

Sutinen, R., **Haavikko, P.** and **Hanninen, P.** (1993) Consistency of Particle size analysis of Geological Earth materials and the effect of sample preparation procedures on reproducibility. *Geol. Surv. Finland Spec. Pap.*, **18**, 63–72.

Tisserand, A., **Malaizé, B.**, **Jullien, E.**, **Zaragosi, S.**, **Charlier, K.** and **Grousset, F.** (2009) African monsoon enhancement during the penultimate glacial period (MIS 6.5 ~ 175 ka) and its atmospheric impact. *Paleoceanagraphy*, **24**, PA2220. doi: 10.1029/2008PA001630

Torrent, J., **Schwertmann, U.**, **Fechter, H.** and **Alferez, F.** (1983) Quantitative relationships between soil color and hematite content. *Soil Sci.*, **136–6**, 354–358.

Trachsel, M., **Grosjean, M.**, **Schnyder, D.**, **Kamenik, C.** and **Rein, B.** (2010) Scanning reflectance spectroscopy (380–730 nm): a novel method for quantitative high resolution climate reconstructions from minerogenic lake sediments. *J. Paleolimnol.*, **44**, 979–994.

Vogel, H., **Meyer-Jacob, C.**, **Melles, M.**, **Brigham-Grette, J.**, **Andreev, A.A.**, **Wennrich, V.** and **Rosén, P.** (2013) Detailed insight into Arctic climatic variability during MIS 11 at Lake El'gygytgyn, NE Russia. *Clim. Past*, **9**, 1467–1479.

Von Gunten, L., **Grosjean, M.**, **Rein, B.**, **Urrutia, R.** and **Appleby, P.** (2009) A quantitative high-resolution summer temperature reconstruction based on sedimentary pigments from Laguna Aculeo, central Chile, back to AD 850. *Holocene*, **19**, 873–881.

Von Gunten, L., **Grosjean, M.**, **Kamenik, C.**, **Fujak, M.** and **Urrutia, R.** (2012) Calibrating biogeochemical and physical climate proxies from non-varved lake sediments with meteorological data: methods and case studies. *J. Paleolimnol.*, **47**, 583–600.

Walker, J.R. (1993) Chlorite polytype geothermometry. *Clay Clay Mineral.*, **41**, 260–267.

Wennrich, B., **Francke, A.**, **Dehnert, A.**, **Juschus, O.**, **Teipe, T.**, **Vogt, C.**, **Brigham-Grette, J.**, **Minyuk, P.S.** and **Melles, M.** (2013) Modern sedimentation patterns of Lake El'gygytgyn, NE Russia, derived from surface sediment and inlet streams samples. *Clim. Past*, **9**, 135–148.

Wolfe, A.P., **Vinebrooke, R.D.**, **Muchelutti, N.**, **Rivard, B.** and **Das, B.** (2006) (2006) Experimental calibration of lake-sediment spectral reflectance to chlorophyll a concentrations: methodology and paleolimnological validation. *J. Paleolimnol.*, **36**, 91–100.

Manuscript received 31 August 2013; revision accepted 6 February 2014